Postprint of: Lange E., Lozano A., Jones N., Hoffmann S., Kumar S., Śmiałek-Telega M., Duflot D., Brunger M., Limão-Vieira P., Absolute Photoabsorption Cross-Sections of Methanol for Terrestrial and Astrophysical Relevance, JOURNAL OF PHYSICAL CHEMISTRY A, Vol. 124, iss. 41 (2020), pp. 8496-8508

Absolute Photoabsorption Cross-Sections of Methanol for Terrestrial and Astrophysical Relevance

E. Lange,[1] A. I. Lozano,[1] N. C. Jones,[2] S. V. Hoffmann,[2] S. Kumar,[1]
M. A. Śmiałek,[3] D. Duflot,[4,5*] M. J. Brunger,[6,7] P. Limão-Vieira,[1*]

[1] Atomic and Molecular Collisions Laboratory, CEFITEC, Department of Physics, Universidade NOVA de Lisboa, 2829-516 Caparica, Portugal

[2] ISA, Department of Physics and Astronomy, Aarhus University, Ny Munkegade 120, DK-8000, Århus C, Denmark

[3] Department of Control and Power Engineering, Faculty of Ocean Engineering and Ship Technology, Gdańsk University of Technology, Gabriela Narutowicza 11/12, 80-233 Gdańsk, Poland

[4] UMR 8523 - Physique des Lasers Atomes et Molécules, Univ. Lille, F-59000 Lille, France

[5] CNRS, UMR 8523, F-59000 Lille, France

[6] College of Science and Engineering, Flinders University, GPO Box 2100, Adelaide, SA 5001, Australia

[7] Dept. of Actuarial Science and Applied Statistics, Faculty of Business and Information Science UCSI, Kuala Lumpur 56000, Malaysia

ABSTRACT

We investigate the methanol absorption spectrum in the range 5.5–10.8 eV in order to provide accurate and absolute cross-sections values. The main goal of this study is to provide a comprehensive analysis of methanol's electronic state spectroscopy by employing high-resolution vacuum ultraviolet (VUV) photoabsorption measurements together with state-of-the art quantum chemical calculation methods. The VUV spectrum reveals several new features that are not previously reported in the literature, for n > 3 in the transitions $\left(ns\sigma(a') \leftarrow (2a'')\right)\left({}^1A' \leftarrow \tilde{X}\,{}^1A'\right)$ and $\left(ns\sigma, np\sigma, np\sigma', nd\sigma \leftarrow (7a')\right)\left({}^1A' \leftarrow \tilde{X}\,{}^1A'\right)$, and with particular relevance to vibrational progressions of the CH_3 rocking mode, $\nu_{11}'(a'')$, mode in the $\left(3p\pi(a'') \leftarrow (2a'')\right)\left(2\,{}^1A' \leftarrow \tilde{X}\,{}^1A'\right)$ absorption band at 8.318 eV. The measured absolute photoabsorption cross sections have subsequently been used to calculate the photolysis lifetime of methanol in the Earth's atmosphere from the ground level up to the limit of the stratosphere (50 km altitude). This shows that solar photolysis plays a negligible role in the

removal of methanol from the lower atmosphere compared with competing sink mechanisms. Torsional potential energy scans, as a function of the internal rotation angle for the ground and first Rydberg states have also been calculated as part of this investigation.

Keywords: methanol, ultraviolet, ISM: molecules, cross-sections, theoretical calculations, Techniques: spectroscopic

* Corresponding authors:
plimaovieira@fct.unl.pt (Paulo Limão-Vieira); denis.duflot@univ-lille.fr (Denis Duflot).

1. INTRODUCTION

Methanol is a relevant organic molecule in the Earth's atmosphere and in the diffuse and dense interstellar medium (ISM).[1–4] It is also considered as a precursor of prebiotic molecules.[5] In the Earth's atmosphere its origin is from natural (e.g. plants),[6] anthropogenic (e.g. biofuel) and biogenic sources (e.g. biomass burning), the latter with an estimated global production of ~4 Tg/y.[7] Lewis et al.[7] have identified that methanol has a relatively short lifetime of 1–12 days, with the main sink mechanisms being attributed to a combination of chemical, photolytic and physical removal processes, while difficult to reconcile with remote location and high-altitude detection. In the different interstellar environments where methanol has been detected, typical abundances relative to H_2 of 10^{-6} to 10^{-7} in hot cores (T ≈ 100–300K), 10^{-9} in dark clouds (T ≈ 10K), and $<10^{-9}$ in diffuse molecular gas have been found.[8,9] As a consequence gas-phase methanol has been considered one of the most abundant interstellar species,[10–12] as well as contributing towards the Orion-IRc2 molecular cloud.[13] Finally, it has also been detected as a trace element in plumes from the geothermally heated south polar region of the geologically active moon of Saturn known as Enceladus.[14]

The chemical reactions for methanol formation in the ISM molecular clouds may include a combination of viable gas-phase and dust grain reactions.[11,15] In the gas-phase,[1] it results from the radiative associative reaction $CH_3^+ + H_2O \rightarrow CH_3OH_2^+ + h\nu$ followed by electronic recombination to CH_3OH (50%) and to H_2CO (50%),[16] whereas on grains a direct surface mechanism through CO hydrogenation has been commonly accepted.[1,5,17] For further details on the physics and chemistry of molecular clouds the interested reader should consult Turner et al.[18] and references therein.

Methanol can be viewed as the result of an hydrogen atom replacement from the water molecule with a methyl group, exhibiting similar character to water[19] but being quite different in terms of position and intensity in its absorption features. CH_3OH has been investigated by various experimental methods that have probed its bond lengths and geometry,[20–22] ultraviolet photoabsorption[22–27] and photodissociation,[28,29] photonionisation[30], photoelectron spectroscopy,[31,32] photoexcitation[33] and electron impact spectroscopies.[31,34,35] As far as UV absorption is concerned, we note that those studies are limited to the wavelength region 120 up to 220 nm (10.332–5.636 eV) despite the general reasonable agreement with the present cross-section values (see Sec. 5.6 for a detailed comparison). Electron-induced chemistry to selected alcohols (and deuterated analogues) has been reported by Ibănescu et al.[36], where Feshbach resonances in the dissociative electron attachment (DEA) spectra (e.g. at 6.53 eV) were compared to the parent Rydberg states in the VUV spectrum (i.e. at 6.768 eV). Electron impact

ionisation and dissociative ionisation of selected biofuels have also been reported on a few occasions by joint experimental and theoretical methods.[37–39] We also note that methanol has been investigated by a number of theoretical methods, with studies including results for its molecular orbitals and geometry[20,21] and calculations on the vertical excitation energies of the neutral molecule.[40]

In this study we present a novel and comprehensive investigation of methanol's electronic state spectroscopy, in a wide photon energy range from 5.5 up to 10.8 eV, combined with state-of-the art calculations, at different levels of theory, for the lowest-lying neutral states. As far as we are aware this constitutes the most accurate assessment of the electronic structure of CH_3OH to date, with the present absolute cross-section values being of relevance for modelling of terrestrial and astrophysical environments.

2. STRUCTURE AND PROPERTIES OF METHANOL

In this section we give a brief summary of the electronic structure of CH_3OH, that is relevant to help us interpreting and assess the role of the main molecular states involved in the excitation features revealed in our photoabsorption spectrum. Methanol is a C_S symmetry molecule in the electronic ground state with bond lengths (Å) and bond angles (°) as listed in Table 1. The calculated electron configuration of the $\tilde{X}\ ^1A'$ ground state is: (a) core orbitals $(1a')^2\ (2a')^2$; (b) valence orbitals $(3a')^2\ (4a')^2\ (5a')^2\ (1a'')^2\ (6a')^2\ (7a')^2\ (2a'')^2$. A close inspection of the ground-state MOs shows that the highest occupied molecular orbital (HOMO), 2a″, is approximately described as the O 2p lone pair orbital perpendicular to the COH plane. On the other hand the second highest (HOMO-1) molecular orbital, 7a′, has the oxygen 2p orbital on the COH plane but away from the direction of the C–O bond (see Supporting Information (SI) Figure S1). Electronic excitations, discussed within the context of this work, are due to the promotion of an electron from the (HOMO) and (HOMO-1) to the valence, Rydberg and mixed character orbitals (see Table 2 for their calculated transition energies and oscillator strengths).

Methanol electronic excitation bands (mainly Rydberg) in the photoabsorption spectrum are accompanied by fine structure assigned to the main fundamental vibrational modes. Their energies (and wavenumbers) in the ground electronic state are 0.456 eV (3681 cm^{-1}) for O–H symmetric stretching, $\nu_1'(a')$, 0.167 eV (1345 cm^{-1}) for C–OH bending, $\nu_6'(a')$, 0.131 eV (1060 cm^{-1}) for CH_3 wagging, $\nu_7'(a')$, and 0.128 eV (1033 cm^{-1}) for CO stretching, $\nu_8'(a')$. Note that for the assignments of the vibronic structure (*X*) we will adopt the notation X_m^n, with *m* and *n* denoting the initial and final vibrational states. The two lowest experimental adiabatic and vertical ionisation energies needed to calculate the quantum defects associated with

transitions to Rydberg orbitals, are here taken from ref.[32] and ref.[31] to be 10.846 $(2a'')^{-1}$ and 12.62 eV $(7a')^{-1}$, respectively. Finally, we note no evidence of dimers contributing to the present spectrum. This result is in line with the absorption spectrum of supersonically expanded beam of methanol, from Sominska and Gedanken,[25] where with no peaks associated with dimers or high oligomers were observed.

3. THEORETICAL METHODS

Assignment of the methanol absorption features has been performed with the aid of *ab initio* calculations results obtained with the MOLPRO package,[41] with our geometry and excitation energies being presented in Tables 1 and 2. The ground state geometry was optimized at the frozen core CCSD(T)[42] level using Dunning's aug-cc-pVQZ atomic basis sets,[43] while the electronic spectra were computed at the EOM-CCSD level[44] at the obtained CCSD(T) geometry. For a better description of the Rydberg excited states, a set of diffuse functions (5s, 5p, 2d), taken from Kaufmann et al.,[45] were added to the original basis set of the O atom (aug-cc-pVQZ+R basis set). Note that the oscillator strengths of the electric dipole transitions were calculated using the length gauge (see Table 2). Additional calculations were also performed using time-dependent density-functional theory (TD-DFT), with the aug-cc-pVQZ+R basis set, on the lowest lying valence singlet states, with those results being compared with previous data in the literature (see Table 3). To this end, the LC-ωPBE functional[46,47] was chosen and the Gaussian 09 code was employed.[48] Finally, in order to help us interpreting the vibrational structure, we used the ezSpectrum code,[49] where the geometries and harmonic frequencies were obtained at the (TD)-B3LYP/aug-cc-pVTZ level and Duschinsky effects were included to account for geometry differences between the states.[50] The BL3YP functional was chosen here because analytical hessian is available. Those latter calculations were undertaken with the Q-Chem code.[51]

4. EXPERIMENTAL METHODS

The high-resolution vacuum ultraviolet (VUV) photoabsorption spectrum of methanol (Figs. 1–3 and Tables 2–7 for corresponding assignments) was recorded at the AU-UV beam line of the ASTRID2 synchrotron facility at Aarhus University, Denmark. The experimental configuration has been described before, so that only the main details are recounted here for the sake of completeness.[52,53] Briefly, monochromatised synchrotron radiation with a resolution of ~0.08 nm, corresponding to 3 meV at the midpoint of the energy range studied passes through a static gas sample that is filled with methanol vapour. Light transmitted through the absorption

cell passes through a transmission window (MgF_2) that sets the lower limit of detection (115 nm), before being detected by a photomultiplier tube (PMT). The methanol sample absolute pressure in the absorption cell is monitored by a capacitance manometer (Chell CDG100D). In order to guarantee the absence of any saturation effects in the data recorded, the absorption cross-sections were carefully measured over the pressure range 0.08–1.30 mbar, with typical attenuations of less than 50%.

Absolute photoabsorption cross-section values (σ in units of Mb ≡ 10^{-18} cm^2) were obtained using the Beer-Lambert attenuation law: $I_t = I_0 e^{(-N\sigma l)}$, where I_t is the light intensity transmitted through the gas sample, I_o is that through the evacuated cell, N the molecular number density of methanol, and l the absorption path length (15.5 cm). The synchrotron beam ring current was monitored throughout the collection of each spectrum and background scans were recorded with the cell evacuated. In order to accurately determine the cross-sections, the VUV spectrum was recorded in small (5 or 10 nm) sections, with at least a 10 points overlap of the adjoining sections. The light intensity at each wavelength is kept quasi-constant through ASTRID2 operating in a "top-up" mode that compensates for the constant beam decay. To compensate for the slight intensity variations (~3%), the incident flux is normalized to the accurately determined beam current in the storage ring. This procedure allows us to determine the accuracy of the present photoabsorption cross-section to within ± 5%.

The liquid sample used in the VUV photoabsorption measurements was purchased from VWR Chemicals, with a stated purity of ≥ 99.8%. That sample was degassed through repeated freeze-pump-thaw cycles.

5. RESULTS AND DISCUSSION

The present absolute high-resolution VUV photoabsorption cross-section of methanol is shown in Figure 1 in the 5.5–10.8 eV photon energy range, with enhanced sections of the same measured cross-section being shown in Figures 2 and 3. The electronic excitation spectrum above 7.5 eV, which is mainly assigned to Rydberg transitions, is rich in fine structure with the C–OH bending mode, v_6', dominant in the energy range 7.5–9.1 eV. In addition, the structure above 9.0 eV is largely due to the overlap of different Rydberg electronic states contributing to the spectrum. In order to avoid congestion in Figure 3, from the different members of the Rydberg series and the fine structure encountered, only a few assignments have been explicitly depicted. Nonetheless, detailed information on all the relevant transitions can be found in Tables 4–6.

The absorption bands of Figures 1–3 are classified as excitations from the ground to mixed valence/Rydberg and mainly Rydberg character (see Section 5.4) states of the type $\left(3s\sigma/\sigma^*(OH) \leftarrow (2a'')\right)$, $\left(3p\sigma(a')/\sigma^*(CH) \leftarrow (7a') + 4p\pi(a'') \leftarrow (2a'')\right)$, $\left(4p\pi(a'') \leftarrow (2a'') + 3p\sigma(a')/\sigma^*(CH) \leftarrow (7a')\right)$, $(ns\sigma, np\sigma, np\pi, np\sigma', nd\sigma, nd\sigma', nd\pi' \leftarrow 2a'')$ and $(ns\sigma, np\sigma, np\sigma', nd\sigma \leftarrow 7a')$. Tables 4–6 show the energy values for the vibrational assignments in the different absorption bands of methanol, and these are compared whenever possible with previous data in the literature. From the high-resolution VUV photoabsorption spectra together with the aid of our theoretical calculations, we therefore now present a comprehensive description of the electronic state spectroscopy of CH_3OH in the different photon energy ranges.

5.1. The 5.5–7.5 eV photon energy range

This energy range (Figure 1) is characterised by a broad weak feature peaking at 6.757 eV which is assigned to a mixed valence/Rydberg $\left(3s\sigma/\sigma^*(OH) \leftarrow (2a'')\right)\left(1\,{}^1A'' \leftarrow \tilde{X}\,{}^1A'\right)$ transition with a local cross-section value of 0.65 Mb (see Table 2). This band has been reported on several previous occasions in experimental[22–24,26–28,33–35,54] and theoretical[40,54] investigations; in particular Wadt et al.[40] reported it at 6.69 eV with an oscillator strength of 1.96×10^{-3}, which is almost half the value obtained in the present calculations, 3.98×10^{-3} (Table 2). Generally speaking most of the authors agree with the maximum cross-section position of this band being at ~ 6.7 eV, although Tsubomura et al.[26] reported it at 7.117 eV.

The calculated electronic radial spatial extent ($<r^2>$) of the lowest-lying singlet transition $\left({}^1A''\right)$in Table 2, gives a value closer to that of the ground state rather than to other members of a Rydberg series, which can be an indication for the more prominent nature of the $\sigma^*_{OH} \leftarrow n_O$ transition (see section 5.4). Furthermore, this band has been also the subject of 185 nm (6.703 eV) photodissociation dynamics studies from Buenker and co-workers.[54] They found that O–H bond breaking proceeds via a strong internal conversion from a 3s Rydberg orbital into a 1s atomic orbital of the hydrogen atom, with no appreciable activation barrier. Such a mechanism indicates a strong avoided crossing involving Rydberg/valence mixing, where the ground-state O–H bond dissociation energy from the calculations of Buenker et al.[54] requires 4.33 eV. Other photodissociation studies includes the work of Satyapal et al.[28] at 193 nm (6.424 eV). Those authors reported that the first absorption band is antibonding in both the O–H and C–O bonds, the former with a quantum yield of $\varphi_H(CH_3OH) = (0.86 \pm 0.10)$, the latter having $\varphi_{OH}(CH_3OH) = (0.75)$. In Table 3, the present EOM-CCSD results are compared with those from previous

MRD-CI calculations of Buenker et al.[54] and the TD-DFT(B3LYP) calculations of Cheng et al.[22] The latter shows a large decrease in the values of the excitation energies with the increasing quality of the basis set. However, the cc-pVNZ (N=T,Q,5) employed by Cheng et al.[22] do not include enough diffuse functions for the appropriate description of the Rydberg states. Thus, the present TD-LC-ωPBE/aug-cc-pVQZ+R values are much closer to those from the EOM-CCSD results in Table 3, compared to those in Cheng et al.[22]

We have performed TD-DFT calculations, with the B3LYP/aug-cc-pVTZ basis set, to obtain the geometry and analytical harmonic frequencies for the low-lying excited states of methanol (n = 3 Rydberg states). Such results are presented in Figures S2–S6 and their related tabulated values in Table S1 (i.e. in the Supporting Information). A close comparison between the 3sσ/σ*(OH) state staggered geometry (Figure S3) and the ground-state staggered (Figure S2) geometry, shows a significant reduction in the O–H stretching mode (88%) while the C–OH bending mode is not so strongly affected (25%). This lends support to the relevant Rydberg/valence nature of the 3sσ/σ*(OH) state, that is nearly dissociated along the O–H coordinate. Franck-Condon factors for the ground to the first excited state transition of methanol were calculated at 300 K, with the result being depicted in Fig. 4. Note that combination bands and hot bands (ν = 1 for both the ground and excited states) were both included in the simulation. The main progression corresponds to the O–H stretching mode, $v_1'(a')$, which is reduced to 0.128 eV in the excited state (Figure S3). This large excitation is to be expected since the 3sσ/σ*(OH) state has a geometry where the OH bond length is increased from about 1.0 to 1.6 Å. Nonetheless, methanol's lowest-lying excited state shows a structureless absorption band with no traces of vibrational excitation in this region (5.5–7.5 eV) of the photoabsorption spectrum. This is mainly due to the superposition of the different modes contributing to the spectrum, where each vibrational peak was convoluted by a Gaussian function with a FWHM of 0.2 eV (Fig. 4, blue solid curve). Note that this value of 0.2 eV was chosen as it best represented the form of the experimental observation. A close inspection of Fig. 4 also reveals that the calculated band exhibits a symmetric shape relative to its maximum value, in some contrast to the experimental data. This is possibly due to the next excited electronic state contributing to the measured absorption band in the high-energy region of the 3sσ/σ*(OH) state. Moreover, Yoshidome et al.[34] measured electron energy-loss spectra and reported the contribution of two $^3A''$ states at 6.3 and 7.5 eV. Although such optically forbidden transitions may not be discernible in the VUV spectrum, the considerable low-intensity of the absorption band at 6.757 eV (0.65 Mb) may also be related to such underlying contributions. The calculated

maximum of the absorption band is located 1.08 eV from that measured. According to the Franck-Condon principle, it should correspond to the adiabatic excitation energy, which is close to the difference between the vertical and adiabatic excitation energies obtained at the TD-B3LYP/aug-cc-pVTZ level (Table S1). Finally, the FWHM of the calculated band (about 0.7 eV), is slightly smaller in magnitude than the value of the observed experimental band (about 0.9 eV).

5.2. The 7.5–9.1 eV photon energy range

The features in this band have been reported upon before,[22,24,31,33,35,40,55] and there is now a fair level of common agreement that they are due to vibronic progressions involving different 3p Rydberg transitions converging to the ionic electronic ground state $(2a'')^{-1}$ of methanol. The measured photoabsorption spectrum is presented in Figure 2, with our proposed assignments summarised in Tables 4 and 5. The current calculations also show that this energy region is mainly characterised by a contribution of Rydberg transitions (see Section 5.4). The lowest-lying vertical excited state of methanol in this energy region is at 7.827 eV, with a local cross-section value of 12.52 Mb. This feature has been assigned to the $\left(3p\sigma(a')/\sigma^*(CH) \leftarrow (2a'')\right)\left(2\ ^1A'' \leftarrow \tilde{X}\ ^1A'\right)$ transition, with an oscillator strength of 0.0305 (Table 2), and shows some fine structure superimposed on a diffuse background reminiscent of the pre-dissociative character of the absorption band. That dissociative nature is in agreement with the 157 nm photodissociation studies of Harich and co-workers,[29] with H elimination not only from the hydroxyl but additionally from the methyl group. The 0_0^0 origin band is tentatively assigned at 7.727 eV (15.78 Mb), in good agreement with the previous values 7.727eV,[22] 7.721 eV[31] and 7.720 eV from Salahub and Sandorfy,[24] although these latter authors have incorrectly labelled it as an (3s ← n) transition. This band also shows a contribution of a 6_0^n (n = 0–2) progression from the C–OH bending mode, $\nu_6'(a')$, with an average spacing of 0.135 eV (1089 cm^{-1}), together with contributions from the CH_3 wagging mode, $\nu_7'(a')$, and C–O stretching , $\nu_8'(a')$, modes (see section 5.4 and Table 4). Here we should not discard the possibility that the C–H in-plane symmetric bending mode, $\nu_5'(a')$, with a calculated value of 0.144 eV (1158 cm^{-1}), can contribute to the spectrum; another progression involving one quantum of the O–H stretching mode, $\nu_1'(a')$, is also discernible at 8.135 eV. It is also worth noting that the mean energy spacing of the $\nu_8'(a')$ mode, 0.099 eV (799 cm^{-1}), is in good agreement with the value from Cheng et al.[22] of 0.100 eV (806 cm^{-1}) and Sominska and Gedanken's[25] value of 0.103 eV (831 cm^{-1}). The calculated geometry and harmonic frequencies for the 3pσ Rydberg state of methanol

are shown in Figure S4 (SI) relative to the ground-state staggered geometry (Figure S2). The 3pσ Rydberg state is now eclipsed, showing a relevant change (increase) in the CH_3 torsion mode ($v'_{12}(a'')$) frequency, together with changes in the frequency values of C–OH bending ($v'_6(a')$), CH_3 wagging ($v'_7(a')$) and O–H stretching ($v'_8(a')$) modes.

The next absorption feature, with the 0_0^0 origin at 8.318 eV, is assigned to the $\left(3p\pi(a'') \leftarrow (2a'')\right)\left(2\ ^1A' \leftarrow \tilde{X}\ ^1A'\right)$ transition. Here we find a calculated an oscillator strength of 0.0277 and a measured cross-section value of 14.4 Mb (Table 2). Note that the present 0_0^0 origin energy is in good agreement with the values of 8.313 eV and 8.321 eV from Cheng et al.[22] and Salahub and Sandorfy.[24] This absorption band is rich in fine structure and accommodates contributions from the CH_3 rocking mode, $v'_{11}(a'')$, with an average spacing of 0.128 eV (1032 cm^{-1}), together with the C–O stretching , $v'_8(a')$, mode (see section 5.4 and Table 4). It is worth mentioning that assignment of the $v'_{11}(a'')$ mode rather than the $v'_6(a')$, mode, with ground-state values of 0.167 (1345 cm^{-1}) and 0.144 eV (1165 cm^{-1}), respectively, results from the good accord with the vibronic features reported in the lowest-lying ionic state in the photoelectron spectrum of Macneil and Dixon[32] and the vibronic structure in the electron energy loss spectrum of Robin and Kuebler.[31] Moreover, the 3pπ Rydberg state eclipsed geometry in Figure S5 (SI), and relative to the ground-state staggered geometry (Figure S2), shows a reduction in the frequency of the CH_3 torsion mode (~50%), while the CH_3 rocking ($v'_{11}(a'')$), CH_3 wagging ($v'_7(a')$) and O–H stretching ($v'_8(a')$) modes are only modestly affected. Note that the C–OH bending ($v'_6(a')$) frequency does not change, which lends support to the unchanged molecular geometry (bent) for the excited state as in the ground state. Such behaviour is also present in the case of the water molecule,[56] which has also been reported by Robin and Kuebler.[31] Another interesting aspect of this absorption band pertains to the possible role of progressions involving the CH_3 rocking mode, $v'_{11}(a'')$, in terms of contributing to the underlying cross section signal, which are here proposed for the first time. The average excited state frequency of the $v'_{11}(a'')$-mode is 0.131 eV (Figure 2) as a result of the 11^n progressions (see Table 5). This is consistent with the MOs in Figure S1 (SI) which are delocalized to the CH_3 group. Cheng et al.[22] reported a single series of the CH_3 torsion mode, $v'_{12}(a'')$, with modest excitation up to 3 quanta, whereas in Figure 2 we can discern at least three series with mean excitation energy of 0.029 eV (234 cm^{-1}) (Table 5) and with a ground-state value of 0.025–0.037 eV (200–295 cm^{-1}).[57] On the other hand the infrared spectrum of Serrallach et al.[20] reported a value of 0.034 eV (271.5 cm^{-1}) from methanol on a Ar-matrix at 15K. However, we

note the relatively low value calculated for the 3pπ Rydberg state of 0.018 eV (146.8 cm^{-1}) in Figure S5.

Another absorption feature with the 0_0^0 origin is at 8.449 eV. This is assigned to the $\left(3p\sigma'(a') \leftarrow (2a'')\right)\left(3\ ^1A'' \leftarrow \tilde{X}\ ^1A'\right)$ transition, with a calculated oscillator strength of 0.0056 and a measured local cross-section value of 14.45 Mb (Table 2.) We note that our 0_0^0 result is in reasonable agreement with the value of 8.313 eV from Cheng et al.[22] The 3pσ′ Rydberg state staggered geometry is shown in Figure S6 (SI) and relative to the ground-state staggered geometry (Figure S2), and shows a reduction in the frequency of the CH_3 rocking mode ($v_{11}'(a'')$) and the O–H stretching ($v_8'(a')$) modes.

Finally, we note two other$\left(3d\sigma(a')/\ \sigma^*(CH) \leftarrow (2a'')\right)\left(4\ ^1A'' \leftarrow \tilde{X}\ ^1A'\right)$ and $\left(3d\sigma'(a') \leftarrow (2a'')\right)\left(5\ ^1A'' \leftarrow \tilde{X}\ ^1A'\right)$ transitions at 8.907 and 9.088 eV. Their measured cross-section values are 4.10 and 6.62 Mb, respectively. The energies of those transitions were previously reported at 8.756 and 8.899 eV by Sominska and Gedanken[25] and at 9.068 eV by Cheng et al.[22] The 3dσ member of the Rydberg series shows evidence of weak contributions from the CH_3 wagging ($v_7'(a')$) mode and the O–H stretching ($v_8'(a')$) mode (see section 5.4 and Table 4).

5.3. The 9.1–10.8 eV photon energy range

This energy range comprises most of the members of the different Rydberg transitions converging to the ionic electronic ground $(2a'')^{-1}$ and first $(7a')^{-1}$ excited states of methanol (Section 5.4), together with fine structure assigned to vibrational excitation. Yet, the calculations in Table 2 also predict mixed transitions which we have assigned to $\left(3p\sigma(a')/\sigma^*(CH/OH) \leftarrow (7a') + 4p\pi(a'') \leftarrow (2a'')\right)$ and $\left(4p\pi(a'') \leftarrow (2a'') + 3p\sigma(a')/\ \sigma^*(CH) \leftarrow (7a')\right)$ at 9.635 and 9.941 eV, in our measured spectrum, and with local cross-section values of 14.84 and 14.70 Mb, respectively. The present spectral assignments are contained in Table 6 with progressions tentatively assigned to the O–H stretching ($v_8'(a')$) mode. The average excited state frequency is 0.118 eV, with a ground-state value of 0.128 eV (1033 cm^{-1}). However, since we have no information about the different geometries of these excited states, an alternative assignment to the fine structure might be the CH_3 rocking mode, $v_{11}'(a'')$, with a ground-state energy of 0.144 eV (1165 cm^{-1}).

5.4. Rydberg transitions

The VUV photoabsorption spectrum above 7.5 eV displays a prominent Rydberg character (Figures 2 and 3), where the experimental energies, proposed assignments and quantum defects

are presented in Table 7. Calculated vertical and adiabatic energies of the lowest-lying 3s and 3p Rydberg states are shown in Table S1 (SI). Each absorption peak position has been tested using the standard Rydberg formula: $E_n = IE - R/(n-\delta)^2$, where *IE* is the ionisation energy, n is the principal quantum number of the Rydberg orbital of energy E_n, R is the Rydberg constant (13.61 eV), and δ is the quantum defect resulting from the penetration of the Rydberg orbital into the core. The Rydberg structures of methanol may have been analysed before,[22,24,25,31–33,35,40,55] but we assert that the present investigation corresponds to the most complete analysis of such states including new series and their assignments being reported here.

The lowest-lying Rydberg transition is assigned to $\left(3s\sigma \leftarrow (2a'')\right)\left(1\,^2A'' \leftarrow \tilde{X}\,^1A'\right)$, with the first member (n = 3) at 6.757 eV and having a quantum defect δ = 1.17. These results are in good agreement with those from Cheng et al.[22] and Robin and Kuebler[31] (Table 7). Note that the slightly larger value of that quantum defect is attributed to a mixed Rydberg/valence character of this electronic transition. Further note that transitions to the Rydberg members n = 4–10, of the $ns\sigma$ series, are reported here for the first time.

The first members of the three n*p* ($np\sigma \leftarrow 2a''$), ($np\pi \leftarrow 2a''$) and ($np\sigma' \leftarrow 2a''$) series are associated with features at 7.727, 8.318 and 8.449 eV (δ = 0.91, 0.68 and 0.62 respectively), and are accompanied by a few quanta of the ν_7' and ν_8'-modes (Table 6). Note that Cheng et al.[22] have earlier reported only two n*p* Rydberg series, assigned as np and np′/np″. The relatively high value of the present quantum defect for the 3pσ Rydberg series member can be attributed to a mixed valence character of the transition, as discussed in Section 5.2. The term values for the 3pσ and 3pπ members are 3.12 and 2.53 (Table 7), while Sominska and Gedanken[25] have comprehensively reported 3.24 and 2.64 and also noted the large value of the former. Tam and Brion[35] place the origin of the transitions at 7.82 and 8.33 eV, with them exhibiting an average vibrational spacing of ~ 0.096 and 0.110 eV. These authors have also noted that the term value for the former band represents an extreme value for a 3p transition. A careful inspection of the npσ′ Rydberg series (Figure 3), shows that some of the higher members (n = 4, 6) have considerably higher intensities that what might be expected as the value of n increases. However, those members are either accompanied by excitation of the ν_7' and ν_8'-modes or as n increases the spectrum becomes more congested so that other members of different Rydberg series are contributing to the absorption features. The assignments in Figure 3 also report the presence of three n*d* ($nd\sigma \leftarrow 2a''$), ($nd\sigma' \leftarrow 2a''$) and ($nd\pi' \leftarrow 2a''$) series associated with the n = 3 peaks at 8.907, 9.088 and 9.238 eV (δ = 0.35, 0.22 and 0.09 respectively). This is in reasonable agreement with the data of Cheng et al.[22] (Table 7). These features are also accompanied by a

few quanta of the ν_7' and ν_8'-modes (Tables 7). Note that for the higher members of the Rydberg series (n > 7), we have not made any attempt to identify features due to their low intensity in the absorption spectrum.

The Rydberg series converging to the ionic electronic first excited state are similarly listed in Table 7, and have been assigned to the $(ns\sigma, np\sigma, np\sigma', nd\sigma \leftarrow 7a')$ $\left(1\,^2A' \leftarrow \tilde{X}\,^1A'\right)$ transitions. The first members of the nsσ, n*p*σ, n*p*σ′ and n*d*σ series are associated with features at 9.38(3) eV (δ =1.17), 9.941 eV (δ =0.75), 10.253 (δ =0.60) and 10.75(0) eV (δ =0.30) (Figure 3 and Table 7). We note that Cheng et al.[22] reported a calculated 3sσ feature at 8.103 eV, although our calculation in Table 2 predicts it to be at 8.904 eV. The latter value is in reasonably good agreement with our experimental finding, given the accuracy of the ab initio method used. The Rydberg tentative assignments of these series have only been made for n = 3, because higher members lie outside the photon energy range investigated, and they appear somewhat broader than usual with such widening being due to contributions from the various vibrational modes (Tables 6).

5.5. Torsional potential energy scans

In the study of the internal rotations of a polyatomic molecule, torsion energy levels and selection rules have been comprehensively discussed by many authors in the past, e.g. ref.[21] and ref.[58], and so that discussion will not be repeated again here. Using the Q-Chem code,[51] we have performed calculations at the B3LYP/aug-cc-pVTZ level of theory for the potential energy scans, V(θ) [cm^{-1}], as a function of the internal rotation angle (θ), by optimizing the geometry of methanol for a fixed value of the torsion angle between the OH and CH bonds. The Fourier expansion of the threefold methanol barrier potential can be given by the analytical expression derived from refs.[21,32,59]:

$$V(\theta) = V_o + V_3(1 - cos3\theta) + V_6(1 - cos6\theta) + V_9(1 - cos9\theta) + V_{12}(1 - cos12\theta) \qquad (1)$$

with the V_0, V_3, V_6, V_9, and V_{12} values and the corresponding torsional potential energy scans, being given in Figures S7–S11 (Supporting Information) for the ground, 3sσ, 3pσ and 3pπ states.

Dai et al.[60] report a ground state barrier (without ZPE correction) of about 340 cm^{-1}, Bowman et al.[59] obtained a value of 342.1 cm^{-1}, while Macneil and Dixon[32] report an internal barrier to rotation of < 400 cm^{-1}. The experimental data of Xu and Hougen[61] yields 373.59 cm^{-1}. These are also in good agreement with the present value of 342 cm^{-1} (Figure S7). The zero-

kinetic energy photoelectron spectroscopy and theoretical calculations of Dai et al.[60] report a 157 cm^{-1} barrier height for the ion, in good agreement with the corresponding result of 150 cm^{-1} from Macneil and Dixon.[32] For the 3s and 3p Rydberg states, our barrier values vary from 141 to 393 cm^{-1} (Figures S8 to S11), with such differences attributed to the spatial extension of the occupied Rydberg orbital which renders rotation to the methyl group.

5.6. Absolute photoabsorption cross sections and atmospheric photolysis

Previous absolute VUV photoabsorption cross sections of methanol are available in the wavelength range 106–198 nm (11.698–6.263 eV),[33] 106–124 nm (11.698–10.000 eV),[30] 107–220 nm (11.589–5.636 eV),[22] 120–200 nm (10.333–6.200 eV),[24] 165–190 nm (7.515–6.526 eV),[26] 165–220 nm (7.515–5.636 eV)[23] and 167–200 nm (7.425–6.200 eV).[27]

Comparing results from those earlier studies with the present, we find Nee et al.[33] report at 173 nm (7.167 eV) a cross-section value of 0.50 Mb which is in reasonable agreement with our value of 0.40 Mb. Similarly, Person and Nicole[30] report at 124 nm (~10 eV) a cross-section value of 15.31 Mb which is excellent accord with the present value of 15.14 Mb. On the other hand, the data of Cheng et al.,[22] Salahub and Sandorfy[24] and Tsubomura et al.[26] for the vertical excitation of the lowest-lying excited state at 6.739 eV, yield cross-sections of 0.61, 0.28 and 0.59 Mb which compare quite favourably with our cross-section value of 0.65 Mb. Two other experimental values from optical absorption experiments report cross-section values at 182.5 nm (6.794 eV) and 184.5 nm (6.720 eV) of 0.619 Mb[23] and 0.57 Mb[27], which also compare quite well against our corresponding results of ~0.65 Mb and 0.65 Mb from the present experiments in Figure 1.

High-resolution VUV absolute photoabsorption cross sections in combination with solar actinic flux measurements from the literature,[62] can be used to calculate the photolysis rates of methanol in the Earth's atmosphere (0–50 km altitude) through a simple methodology, as described in ref. [63]. The quantum yield for dissociation, either in H-atom release from OH or OH from CH_3, is taken as 0.86 and 0.75 respectively, from the work of Satyapal et al.[28] Photolysis lifetimes of less than 2 weeks sunlit day were calculated at altitudes above 40 km. This indicates that methane molecules can be efficiently broken up by VUV absorption at these altitudes. At lower altitudes, however, the photolysis lifetimes are very high, meaning that these molecules cannot be efficiently broken up by UV radiation. Liu et al.[64] and Gao et al.[65] reported a comprehensive study of the gas-phase kinetics for the CH_3OH + OH reaction, as a function of the temperature, finding rate values at room temperature of $k_{OH} = 8.68\times10^{-13}$ cm^3 $molecule^{-1}$ s^{-1} and $k_{OH} = 8.02\times10^{-13}$ cm^3 $molecule^{-1}$ s^{-1}, respectively. MacDonald and Fall[6] have also

reported that methanol reactions with atmospheric OH radicals have relatively low rate values. Yet, the reaction of methanol with OH yields CH_2O (formaldehyde, which is highly reactive in the atmosphere) and the HO_2 radical, which may then participate in the formation of tropospheric ozone.[6]

Thus, compared with these alternative reaction pathways, UV photolysis is not expected to play a significant role in the tropospheric removal of CH_3OH molecules, which has also been recognised by Lewis et al.[7] despite their atmospheric lifetime being calculated only with respect to OH local chemical reactions. Moreover, Lewis et al.[7] have identified that in the North Atlantic marine air, acetaldehyde, methanol and acetone make up to 80% of the main sink mechanism of OH radicals in that atmosphere, while the lifetime with respect to oceanic destruction is roughly similar to that due to atmospheric OH concentration.

6. CONCLUSIONS

We have reported the most up to date and comprehensive investigation into the VUV electronic spectroscopy of methanol in the 5.5–10.8 eV range, with the complete set of absolute photoabsorption cross-sections in this region being presented. These data are of relevance for modelling the role of methanol in the Earth's atmosphere, as well as in the Lyman-α region of the diffuse and dense interstellar medium. The absorption bands were classified as excitations from the ground to mixed valence/Rydberg and mainly Rydberg character states, with novel assignments in the photon energy covered in this work which have not been previously reported in the literature, being made. Theoretical calculations on the vertical excitation energies and oscillator strengths were performed using the equation-of-motion coupled cluster method, restricted to the single and double excitations level (EOM-CCSD), to help us in assigning the valence and Rydberg transitions.

As just noted the VUV spectrum revealed several new features that have not previously been reported in the literature, $\left(ns\sigma, np\sigma, np\sigma', nd\sigma \leftarrow (7a')\right)\left({}^1A' \leftarrow \tilde{X}\ {}^1A'\right)$, with particular attention being given to the n > 3 members of the Rydberg $\left(ns\sigma(a') \leftarrow (2a'')\right)\left({}^1A' \leftarrow \tilde{X}\ {}^1A'\right)$ transitions, as well as to the vibrational progressions of the $\left(3p\pi(a'') \leftarrow (2a'')\right)\left(2\ {}^1A' \leftarrow \tilde{X}\ {}^1A'\right)$ absorption band at 8.318 eV. The analysis of these structures in the photoabsorption spectra has also allowed us to propose, again for the first-time, assignments for the CH_3 rocking mode, $v'_{11}(a'')$, mode. Torsional potential energy scans, as a function of the internal rotation angle for the ground and first Rydberg states, were calculated at the TD-DFT level of theory with a B3LYP/aug-cc-pVTZ basis set. Finally, the photolysis lifetimes of methanol were also

obtained for the Earth's troposphere and stratosphere, and showed that solar photolysis is not expected to be a sink in the lower terrestrial atmosphere.

AUTHOR INFORMATION

Corresponding Authors

(P.L.-V.) E-mail: plimaovieira@fct.unl.pt; (D.D.) E-mail: denis.duflot@univ-lille.fr

ORCID

E. Lange: 0000-0002-9279-8210

N. C. Jones: 0000-0002-4081-6405

S. V. Hoffmann: 0000-0002-8018-5433

A. I. Lozano: 0000-0003-4613-0372

S. Kumar: 0000-0002-1996-9925

M. A. Śmiałek: 0000-0003-2624-3716

D. Duflot: 0000-0002-8307-5344

M. J. Brunger: 0000-0002-7743-2990

P. Limão-Vieira: 0000-0003-2696-1152

Notes

The authors declare no competing financial interest.

Supporting Information

See supporting Information for the shape of a selection of methanol molecular orbitals, the geometry of the ground and lowest-lying Rydberg states and the related torsional potential energy scans.

ACKNOWLEDGMENTS

E.L. acknowledges the Brazilian Agency Conselho Nacional de Desenvolvimento Científico e Tecnológico (CNPq) and the Science Without Borders Programme for opportunities to study abroad. S.K. acknowledges the Portuguese National Funding Agency FCT through Researcher PD/BD/142831/2018, and, together with A.I.L. and P.L.V., the Research Grants CEFITEC (UIDB/00068/2020) and PTDC/FIS-AQM/31281/2017. This work was also supported by the Radiation Biology and Biophysics Doctoral Training Programme (RaBBiT, PD/00193/2012); UCIBIO (UIDB/04378/2020). The research leading to these results has received funding from

the European Community's Seventh Framework Programme CalipsoPlus (FP7/2007-2013) under grant agreement nº 226716. DD acknowledges the support of the OVERSEE and CAPPA grants, managed by the Agence Nationale de la Recherche under the frame programs Investissements d'Avenir ANR-10-LABX-005 and I-SITE ULNE/ANR-16-IDEX-0004 ULNE, respectively. D.D. also thanks the Région Hauts de France, the Ministère de l'Enseignement Supérieur et de la Recherche (CPER Climibio) and the European Fund for Regional Economic Development for their support. This work used HPC resources from GENCITGCC (Grant No. 2020-A0070801859) and the Centre de Ressources Informatiques (CRI) of the Université de Lille. Partial financial support from the Australian Research Council through grant DP180101655 is also acknowledged.

REFERENCES

(1) Turner, B. E. The Physics and Chemistry of Small Translucent Molecular Clouds. XI . Methanol. *Astrophys. J.* **1998**, *501*, 731–748.

(2) Mann, A. P. C.; Williams, D. A. A List of Interstellar Molecules. *Nature* **1980**, *283*, 721–725.

(3) Ball, J. A.; Gottlieb, C. A.; Lilley, A. E. Detection of Methyl Alcohol in Sagittarius. *Astrophys. J.* **1970**, *162*, L203–L210.

(4) Whittet, D. C. B.; Cook, A. M.; Herbst, E.; Chiar, J. E.; Shenoy, S. S. Observational Constraints on Methanol Production in Interstellar and Preplanetary Ices. *Astrophys. J.* **2011**, *742* (1).

(5) Walsh, C.; Loomis, R. A.; Öberg, K. I.; Kama, M.; van 't Hoff, M. L. R.; Millar, T. J.; Aikawa, Y.; Herbst, E.; Widicus Weaver, S. L.; Nomura, H. First Detection of Gas-Phase Methanol in a Protoplanetary Disk. *Astrophys. J. Lett.* **2016**, *823*, L10.

(6) MacDonald, R. C.; Fall, R. Detection of Substantial Emissions of Methanol from Plants to the Atmosphere. *Atmos. Environ.* **1993**, *27*, 1709–1713.

(7) Lewis, A. C.; Hopkins, J. R.; Carpenter, L. J.; Stanton, J.; Read, K. A.; Pilling, M. J. Sources and Sinks of Acetone, Methanol, and Acetaldehyde in North Atlantic Air. *Atom. Chem. Phys.* **2005**, *5*, 1963–1974.

(8) Liszt, H. S.; Pety, J.; Lucas, R. Limits on Chemical Complexity in Diffuse Clouds: Search for CH_3OH and HC_5N Absorption. *Astron. Astrophys.* **2008**, *486*, 493–496.

(9) Wirström, E. S.; Geppert, W. D.; Hjalmarson, Å.; Persson, C. M.; Black, J. H.; Bergman, P.; Millar, T. J.; Hamberg, M.; Vigren, E. Observational Tests of Interstellar Methanol Formation. *Astron. Astrophys.* **2011**, *533*, 1–11.

(10) Garrod, R.; Hee Park, I.; Caselli, P.; Herbst, E. Are Gas-Phase Models of Interstellar Chemistry Tenable? The Case of Methanol. *Faraday Discuss.* **2006**, *133*, 51–62.

(11) Gamez-Garcia, V. G.; Galano, A. Systematic Search for Chemical Reactions in Gas Phase Contributing to Methanol Formation in Interstellar Space. *J. Phys. Chem. A* **2017**, *121*, 7393–7400.

(12) Charnley, S. B.; Kress, M. E.; Tielens, A. G. G. M.; Millar, T. J. Interstellar Alcohols. *Astrophys. J.* **1995**, *448*, 232–239.

(13) Jacq, T.; Walmsley, C. M.; Mauersberger, R.; Anderson, T.; Herbst, E.; De Lucia, F. C. Detection of Interstellar CH_2DOH. *Astron. Astrophys.* **1993**, *271*, 276–281.

(14) Spencer, J. R.; Barr, A. C.; Esposito, L. W.; Helfenstein, P.; Ingersoll, A. P.; Jaumann, R.; Christopher P. McKay, F. N.; Waite, J. H. Enceladus: An Active Cryovolcanic

Satellite. In *Saturn from Cassini-Huygens*; M. K., D., L. W., E., Krimigis, S. M., Eds.; 2009; pp 683–724.

(15) Bergantini, A.; Maksyutenko, P.; Kaiser, R. I. On the Formation of the C_2H_6O Isomers Ethanol (C_2H_5OH) and Dimethyl Ether (CH_3OCH_3) in Star-Forming Regions. *Astrophys. J.* **2017**, *841*, 96.

(16) Lee, H. H.; Bettens, R. P. A.; Herbst, E. Fractional Abundances of Molecules in Dense Interstellar Clouds: A Compendium of Recent Model Results. *Astron. Astrophys. Suppl. Ser.* **1996**, *119*, 111–114.

(17) Viti, S.; Williams, D. A.; O'Neill, P. T. Hydrocarbons in Diffuse and Translucent Clouds. *Astron. Astrophys.* **2000**, *354*, 1062–1070.

(18) Turner, B. E.; Herbst, E.; Terzieva, R. The Physics and Chemistry of Small Translucent Molecular Clouds. XIII. The Basic Hydrocarbon Chemistry. *Astrophys. J. Suppl. S.* **2000**, *126*, 427–460.

(19) Wei, J.; Karpichev, B.; Reisler, H. Unimolecular Processes in CH_2OH below the Dissociation Barrier: O-H Stretch Overtone Excitation and Dissociation. *J. Chem. Phys.* **2006**, *125*, 034303.

(20) Serrallach, A.; Meyer, R.; Günthard, H. H. Methanol and Deuterated Species: Infrared Data, Valence Force Field, Rotamers, and Conformation. *J. Mol. Spectrosc.* **1974**, *52*, 94–129.

(21) Lees, R. M.; Baker, J. G. Torsion-Vibration-Rotation Interactions in Methanol. I. Millimeter Wave Spectrum. *J. Chem. Phys.* **1968**, *48*, 5299–5318.

(22) Cheng, B. M.; Bahou, M.; Chen, W. C.; Yui, C. H.; Lee, Y. P.; Lee, L. C. Experimental and Theoretical Studies on Vacuum Ultraviolet Absorption Cross Sections and Photodissociation of CH_3OH, CH_3OD, CD_3OH, and CD_3OD. *J. Chem. Phys.* **2002**, *117*, 1633–1640.

(23) Cheng, B. M.; Bahou, M.; Lee, Y. P.; Lee, L. C. Absorption Cross Sections and Solar Photodissociation Rates of Deuterated Isotopomers of Methanol. *J. Geophys. Res.* **2002**, *107*, 1161.

(24) Salahub, D. R.; Sandorfy, C. The Far-Ultraviolet Spectra of Some Simple Alcohols and Fluoroalcohols. *Chem. Phys. Lett.* **1971**, *8*, 71–74.

(25) Sominska, E.; Gedanken, A. The Absorption Spectrum of a Supersonically Expanded Beam of Methanol in the Vacuum Ultraviolet Region. *J. Mol. Spectrosc.* **1996**, *175* (2), 234–238.

(26) Tsubomura, H.; Kimura, K.; Kaya, K.; Tanaka, J.; Nagakura, S. Vacuum Ultraviolet

Absorption Spectra of Saturated Organic Compounds with Non-Bonding Electrons. *B. Chem. Soc. Jpn.* **1964**, *37*, 417–423.

(27) Harrison, A. J.; Cederholm, B. J.; Terwilliger, M. A. Absorption of Acyclic Oxygen Compounds in the Vacuum Ultraviolet. III. Acetone and Acetaldehyde. *J. Chem. Phys.* **1959**, *30*, 355–356.

(28) Satyapal, S.; Park, J.; Bersohn, R.; Katz, B. Dissociation of Methanol and Ethanol Activated by a Chemical Reaction or by Light. *J. Chem. Phys.* **1989**, *91* (11), 6873–6879.

(29) Harich, S.; Lin, J. J.; Lee, Y. T.; Yang, X. Competing Atomic and Molecular Hydrogen Pathways in the Photodissociation of Methanol at 157 nm. *J. Chem. Phys.* **1999**, *111*, 5–9.

(30) Person, J. C.; Nicole, P. P. Isotope Effects in the Photoionization Yields and the Absorption Cross Sections for Ethylene and N-Butane. *J. Chem. Phys.* **1971**, *55*, 3390–3397.

(31) Robin, M. B.; Kuebler, N. A. Excited Electronic States of the Simple Alcohols. *J. Electron Spectrosc. Relat. Phenom.* **1972**, *1*, 13–28.

(32) Macneil, K. A. G.; Dixon, R. N. High Resolution Photoelectron Spectroscopy of Methanol and Its Deuterated Derivatives: Internal Rotation in the Ground Ionic State. *J. Electron Spectrosc. Relat. Phenom.* **1977**, *11*, 315–331.

(33) Nee, J. B.; Suto, M.; Lee, L. C. Photoexcitation Processes of CH3OH: Rydberg States and Photofragment Fluorescence. *Chem. Phys.* **1985**, *98*, 147–155.

(34) Yoshidome, T.; Kawazumi, H.; Ogawa, T. Electron Energy-Loss Spectra of Methanol and Assignments of Its Triplet States. *J. Electron Spectrosc. Relat. Phenom.* **1990**, *53*, 185–192.

(35) Tam, W.-C.; Brion, C. E. Electron Impact Spectra of Some Alkyl Derivatives of Water and Related Compounds. *J. Electron Spectrosc. Relat. Phenom.* **1974**, *3*, 263–279.

(36) Ibănescu, B. C.; May, O.; Monney, A.; Allan, M. Electron-Induced Chemistry of Alcohols. *Phys. Chem. Chem. Phys.* **2007**, *9*, 3163–3173.

(37) Nixon, K. L.; Pires, W. A. D.; Neves, R. F. C.; Duque, H. V.; Jones, D. B.; Brunger, M. J.; Lopes, M. C. A. Electron Impact Ionisation and Fragmentation of Methanol and Ethanol. *Int. J. Mass Spectrom.* **2016**, *404*, 48–59.

(38) Brunger, M. J. Electron Scattering and Transport in Biofuels, Biomolecules and Biomass Fragments. *Int. Rev. Phys. Chem.* **2017**, *36*, 333–376.

(39) Lopes, M. C. A.; Pires, W. A. D.; Nixon, K. L.; Amorim, R. A. A.; da Silva, D. G. M.;

Fernandes, A. C. P.; Ghosh, S.; Jones, D. B.; Campbell, L.; Neves, R. F. C.; et al. Electron Impact Ionization and Fragmentation of Biofuels. *Eur. Phys. J. D* **2020**, *74*, 88.

(40) Wadt, W. R.; Iii, W. A. G. The Low-Lying Excited States of Water, Methanol and Dimethyl Ether. *Chem. Phys.* **1976**, *18*, 1–11.

(41) Werner, H.-J.; Knowles, P. J.; Knizia, G.; Manby, F. R.; Schütz, M.; Celani, P.; Györffy, W.; Kats, D.; Korona, T.; Lindh, R.; et al. MOLPRO, Version 2015.1. MOLPRO, 2015.1, a package of ab initio programs 2015.

(42) Watts, J. D.; Gauss, J.; Bartlett, R. J. Coupled-Cluster Methods with Noniterative Triple Excitations for Restricted Open-Shell Hartree-Fock and Other General Single Determinant Reference Functions. Energies and Analytical Gradients. *J. Chem. Phys.* **1993**, *98*, 8718–8733.

(43) Wilson, A. K.; van Mourik, T.; Dunning Jr., T. H. Sextuple Zeta Correlation Consistent Basis Sets for Boron through Neon. *Comp. Theor. Chem.* **1996**, *388*, 339–349.

(44) Korona, T.; Werner, H. J. Local Treatment of Electron Excitations in the EOM-CCSD Method. *J. Chem. Phys.* **2003**, *118*, 3006–3019.

(45) Kaufmann, K.; Baumeister, W.; Jungen, M. Universal Gaussian Basis Sets for an Optimum Representation of Rydberg and Continuum Wavefunctions. *J. Phys. B At. Mol. Opt. Phys.* **1989**, *22*, 2223–2240.

(46) Vydrov, O. A.; Scuseria, G. E.; Perdew, J. P. Tests of Functionals for Systems with Fractional Electron Number. *J. Chem. Phys.* **2007**, *126*, 154109.

(47) Vydrov, O. A.; Scuseria, G. E. Assessment of a Long-Range Corrected Hybrid Functional. *J. Chem. Phys.* **2006**, *125*, 234109.

(48) Frisch, M. J.; Trucks, G. W.; Schlegel, H. B.; Scuseria, G. E.; Robb, M. A.; Cheeseman, J. R.; Scalmani, G.; Barone, V.; Mennucci, B.; Petersson, G. A.; et al. Gaussian 09. Wallingford, CT, USA 2009.

(49) Mozhayskiy, V. A.; Krylov, A. I. ezSpectrum 3.0 http://iopenshell.usc.edu/downloads.

(50) Duschinsky, F. The Importance of the Electron Spectrum in Multi Atomic Molecules. Concerning the Franck-Condon Principle. *Acta Physicochim. URSS* **1937**, *7*, 551–566.

(51) Shao, Y.; Gan, Z.; Epifanovsky, E.; Gilbert, A. T. B.; Wormit, M.; Kussmann, J.; Lange, A. W.; Behn, A.; Deng, J.; Feng, X.; et al. Advances in Molecular Quantum Chemistry Contained in the Q-Chem 4 Program Package. *Mol. Phys.* **2015**, *113*, 184–215.

(52) Eden, S.; Limão-Vieira, P.; Hoffmann, S. V.; Mason, N. J. VUV Photoabsorption in

CF_3X (X = Cl, Br, I) Fluoro-Alkanes. *Chem. Phys.* **2006**, *323*, 313–333.

(53) Palmer, M. H.; Ridley, T.; Hoffmann, S. V.; Jones, N. C.; Coreno, M.; De Simone, M.; Grazioli, C.; Biczysko, M.; Baiardi, A.; Limão-Vieira, P. Interpretation of the Vacuum Ultraviolet Photoabsorption Spectrum of Iodobenzene by Ab Initio Computations. *J. Chem. Phys.* **2015**, *142*, 134302.

(54) Buenker, R. J.; Olbrich, G.; Schuchmann, H. P.; Schumann, B. L.; von Sonntag, C. Photolysis of Methanol at 185 nm. Quantum Mechanical Calculations and Product Study. *J. Am. Chem. Soc.* **1984**, *106*, 4362–4368.

(55) Robin, M. B. *Higher Excited States of Polyatomic Molecules, Volume I*; Academic Press, 1974.

(56) Mota, R.; Parafita, R.; Giuliani, A.; Hubin-Franskin, M.-J.; Lourenço, J. M. C.; Garcia, G.; Hoffmann, S. V.; Mason, N. J.; Ribeiro, P. A.; Raposo, M.; et al. Water VUV Electronic State Spectroscopy by Synchrotron Radiation. *Chem. Phys. Lett.* **2005**, *416*, 152–159.

(57) Shimanouchi, T. *Tables of Molecular Vibrational Frequencies Consolidated Volume I*; National Bureau of Standards, 1972.

(58) Rueda, D.; Boyarkin, O. V.; Rizzo, T. R.; Mukhopadhyay, I.; Perry, D. S. Torsion-Rotation Analysis of OH Stretch Overtone-Torsion Combination Bands in Methanol. *J. Chem. Phys.* **2002**, *116*, 91–100.

(59) Bowman, J. M.; Huang, X.; Handy, N. C.; Carter, S. Vibrational Levels of Methanol Calculated by the Reaction Path Version of MULTIMODE, Using an Ab Initio, Full-Dimensional Potential. *J. Phys. Chem. A* **2007**, *111*, 7317–7321.

(60) Dai, Z.; Gao, S.; Wang, J.; Mo, Y. Torsional Energy Levels of $CH_3OH^+/CH_3OD^+/CD_3OD^+$ Studied by Zero-Kinetic Energy Photoelectron Spectroscopy and Theoretical Calculations. *J. Chem. Phys.* **2014**, *141*, 144306.

(61) Xu, L. H.; Hougen, J. T. Global Fit of Torsion-Rotation Transitions in the Ground and First Excited Torsional States of Methanol. *J. Mol. Spectrosc.* **1995**, *173*, 540–551.

(62) *Chemical Kinetics and Photochemical Data for Use in Stratospheric Modelling, Evaluation Number 12, NASA, Jet Propulsion Laboratory, JPL, Publication 97-4, January 15*; 1997.

(63) Limão-Vieira, P.; Eden, S.; Kendall, P. A.; Mason, N. J.; Hoffmann, S. V. VUV Photo-Absorption Cross-Section for CCl_2F_2. *Chem. Phys. Lett.* **2002**, *364*, 535–541.

(64) Liu, D.; Giri, B. R.; Farooq, A. A Shock Tube Kinetic Study on the Branching Ratio of Methanol + OH Reaction. *P. Combust. Inst.* **2019**, *37*, 153–162.

(65) Gao, L. G.; Zheng, J.; Fernández-Ramos, A.; Truhlar, D. G.; Xu, X. Kinetics of the Methanol Reaction with OH at Interstellar, Atmospheric, and Combustion Temperatures. *J. Am. Chem. Soc.* **2018**, *140*, 2906–2918.

Figure captions

Fig. 1. The present high-resolution VUV photoabsorption spectrum of CH_3OH in the 5.5–10.8 eV photon energy range. See text for details.

Fig. 2. An enhanced plot for the VUV photoabsorption spectrum of CH_3OH in the 7.5–9.2 eV photon energy range. See text for details.

Fig. 3. An expanded plot for the VUV photoabsorption spectrum of CH_3OH in the 9.0–10.8 eV photon energy range. See text for details.

Fig. 4. The present Franck-Condon factors calculated for the CH_3OH first absorption band, together with their superposition weighted by Boltzmann factors (the red line is the actual photoabsorption spectrum which is displaced to avoid congesting the figure); geometry and harmonic frequencies calculated at (TD)-B3LYP/aug-cc-pVTZ level. Note that the photon energy for the maximum of the calculated band has been set to match the experimental one. See text for details.

Table caption

Table 1. Present calculated geometry of CH_3OH compared with corresponding results from previous works. Bond lengths are in Å and bond angles in (°).

Table 2. The calculated vertical excitation energies (EOM-CCSD/aug-cc-pVQZ+R) and oscillator strengths of CH_3OH, compared where possible with corresponding experimental data (energies in eV). See text for details.

Table 3. The calculated vertical excitation energies of CH_3OH, compared with our experimental data and the results from previous work (energies in eV). See text for details.

Table 4. Proposed vibrational assignments of the CH_3OH absorption bands in the photon energy range 7.5−9.1 eV[a]. Energies in eV.

Table 5. Proposed assignments of vibrational progressions in CH_3OH absorption bands in the photon energy range 8.2−8.9 eV[a]. Energies in eV.

Table 6. Proposed assignments of vibrational progressions in CH_3OH absorption bands in the photon energy range 9.0−10.8 eV[a]. Energies in eV.

Table 7. Energy values (eV), quantum defects (δ) and our assignments of the Rydberg series converging to the ionic electronic ground $(2a'')^{-1}$ and first $(7a')^{-1}$ excited states of methanol, CH_3OH[a].

Fig. 1. The present high-resolution VUV photoabsorption spectrum of CH_3OH in the 5.5–10.8 eV photon energy range. See text for details.

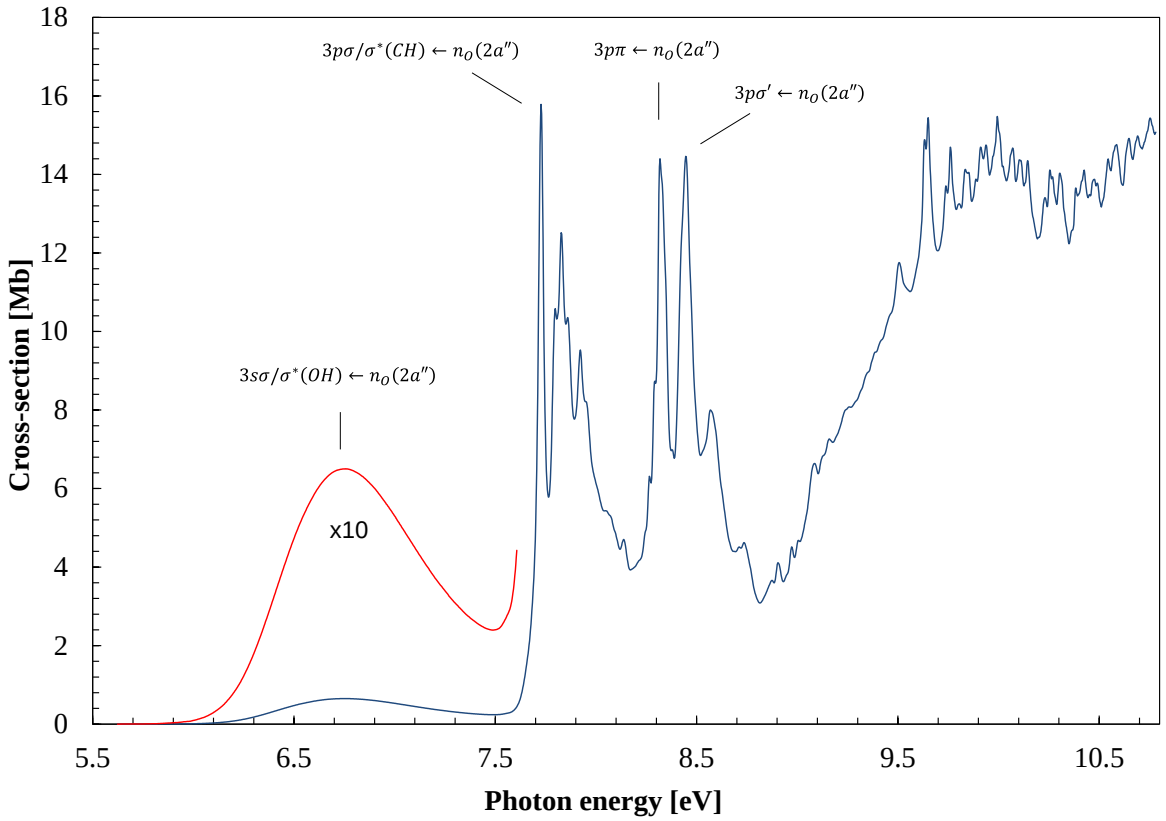

Fig. 2. An enhanced plot for the VUV photoabsorption spectrum of CH_3OH in the 7.5–9.2 eV photon energy range. See text for details.

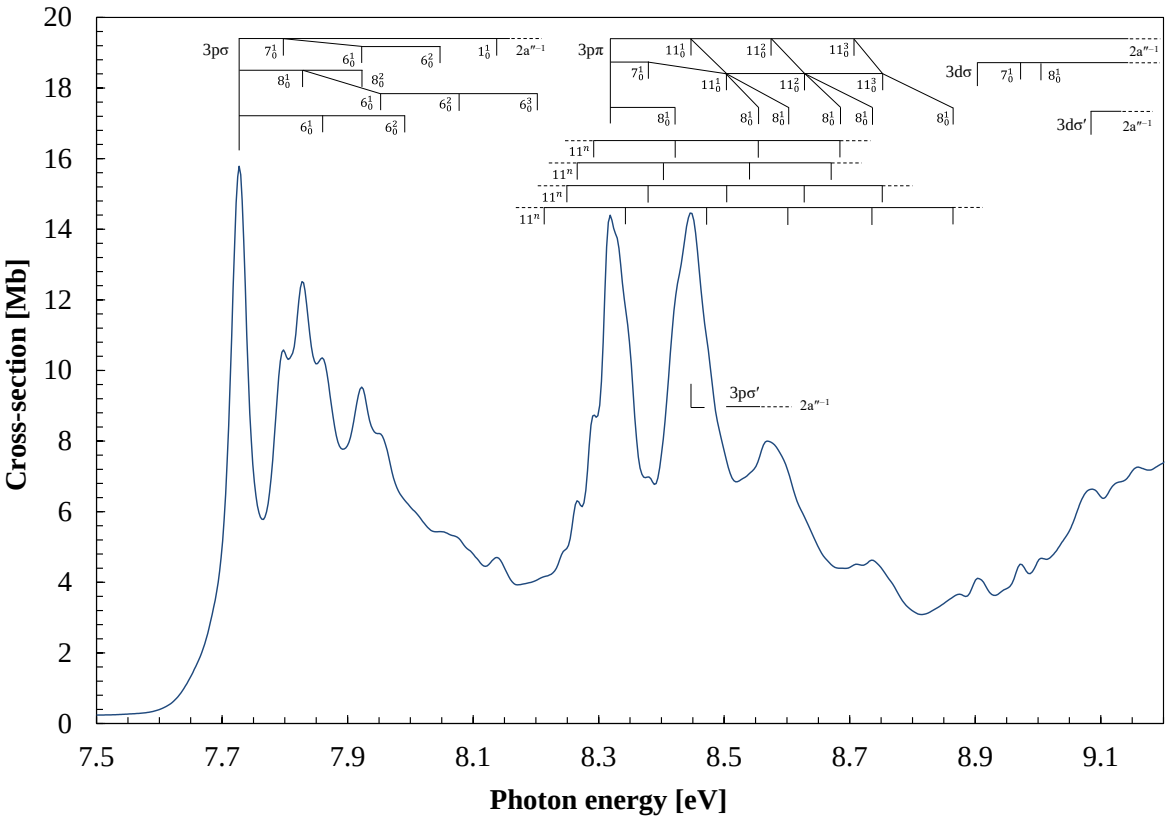

Fig. 3. An expanded plot for the VUV photoabsorption spectrum of CH_3OH in the 9.0–10.8 eV photon energy range. See text for details.

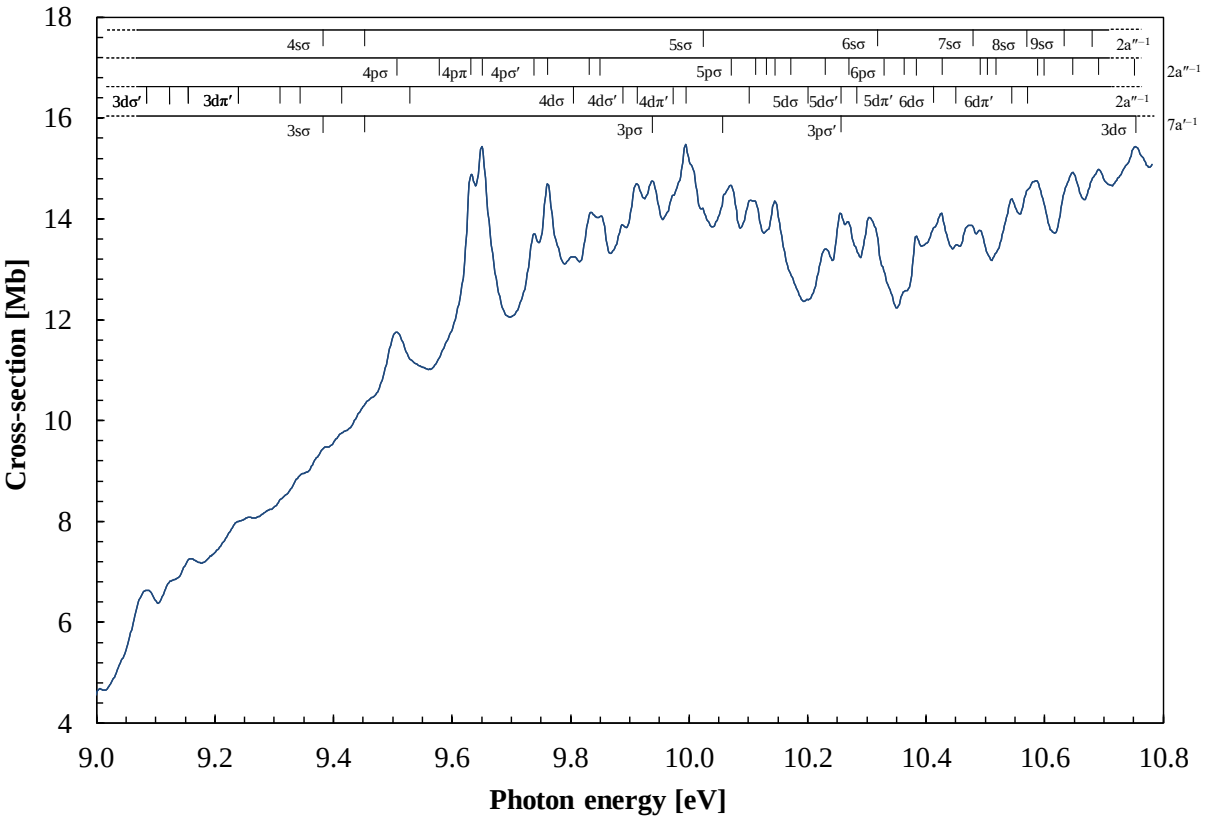

Fig. 4. The present Franck-Condon factors calculated for the CH_3OH first absorption band, together with their superposition weighted by Boltzmann factors (the red line is the actual photoabsorption spectrum which is displaced to avoid congesting the figure); geometry and harmonic frequencies calculated at (TD)-B3LYP/aug-cc-pVTZ level. Note that the photon energy for the maximum of the calculated band has been set to match the experimental one. See text for details.

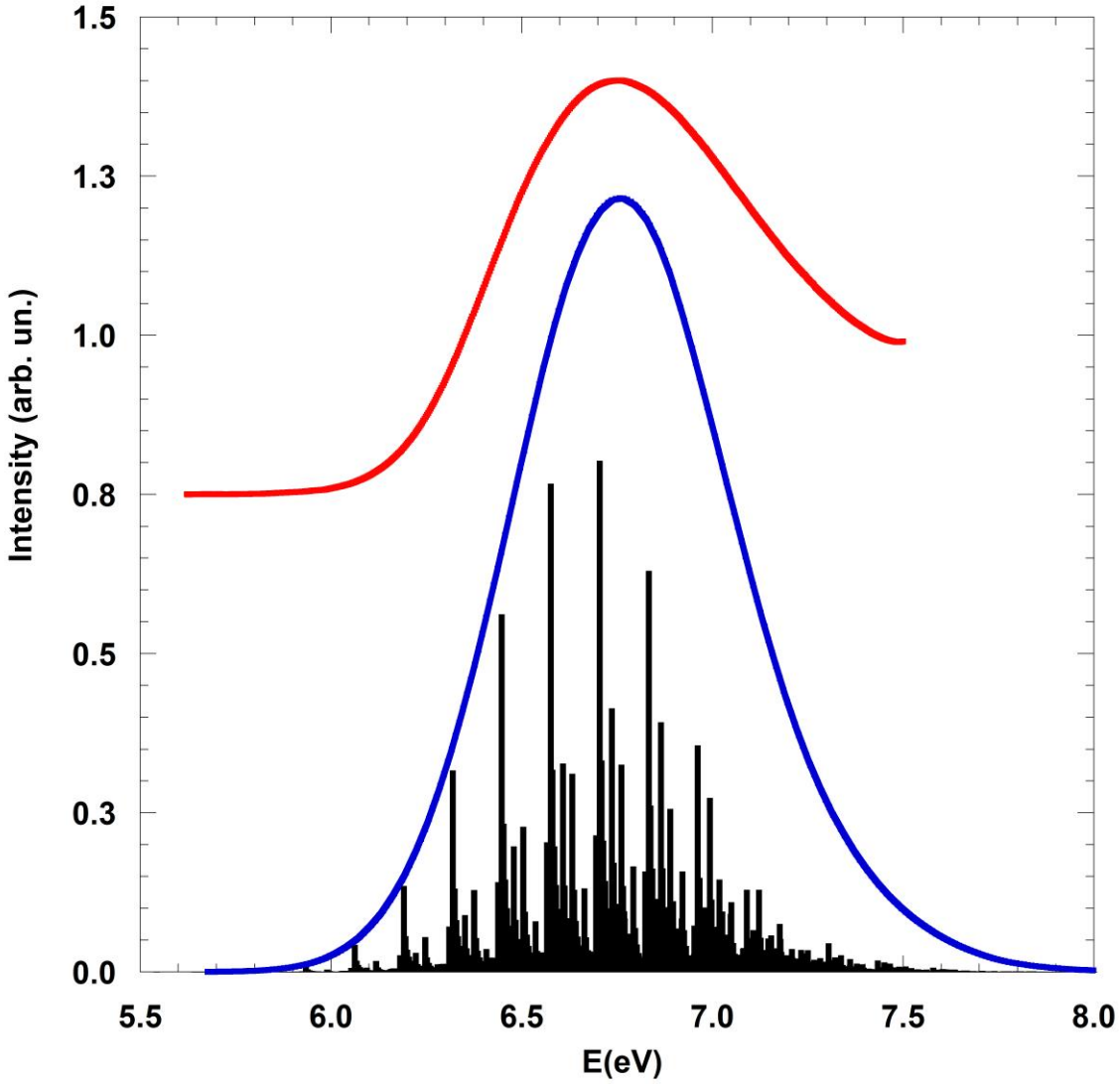

Table 1. Present calculated geometry of CH_3OH compared with corresponding results from previous works. Bond lengths are in Å and bond angles in (°).

	This work	Theory ref.[22]	Exp. ref.[20]	Exp. ref.[21]
	CCSD(T) aug-cc-pVQZ	B3LYP cc-pV5Z		
R(CH) (in-plane)	1.0877	1.087	1.093	1.0936
R(CH) (out-of-plane, two bonds)	1.0904	1.094		
R(CO)	1.4191	1.421	1.424	1.4246
R(OH)	0.9585	0.959	0.945	0.9451
∡ COH	108.2	109.04	108.32	108.32
∡ HCO (in-plane)	106.8	106.81	110.18	–
∡ HCO (out-of-plane)	111.9	112.12		–
∡ HCH	109.2	–	108.38	108.38

Table 2. The calculated vertical excitation energies (EOM-CCSD/aug-cc-pVQZ+R) and oscillator strengths of CH_3OH, compared where possible with corresponding experimental data (energies in eV). See text for details.

State	E (eV)	f_L	$<r^2>^a$	HOMO (2a″)	HOMO-1 (7a′)	Mixed character	E (eV) expt.	Cross-section (Mb)
$\tilde{X}\ ^1A'$			29					
$^1A''$	6.948	0.00398	49	3sσ/σ*(OH)			6.757	0.65
$^1A''$	8.136	0.03050	72	3pσ(a′)/σ*(CH)			7.727	15.78
$^1A'$	8.573	0.02765	84	3pπ(a″)			8.318	14.40
$^1A''$	8.592	0.00562	81	3pσ′(a′)			8.449	14.45
$^1A'$	8.904	0.00126	51		3sσ/σ*(OH)		9.38(3)	9.45
$^1A''$	9.197	0.00046	123	3dσ(a′)/σ*(CH/OH)			8.907	4.10
$^1A''$	9.365	0.00163	112	3dσ′(a′)			9.088	6.62
$^1A'$	9.472	0.00060	120	3dπ(a″)				
$^1A''$	9.505	0.00061	156	3dσ″(a′)				
$^1A''$	9.610	0.00012	163	3dσ(a′)/σ*				
$^1A'$	9.619	0.00132	158	3dπ′(a″)			9.238	7.99
$^1A''$	9.738	0.00506	269	4sσ(a′)			9.38(3)	9.45
$^1A'$	9.833	0.05598	141			HOMO-1 → 3pσ(a′)/σ*(CH) + HOMO → 4pπ(a″)	9.635	14.84
$^1A''$	9.872	0.00089	304	4pσ(a′)			9.50(2)	11.71
$^1A'$	9.888	0.01220	243			HOMO → 4pπ(a″) + HOMO-1 → 3pσ(a′)/σ*(CH)	9.941	14.70
$^1A''$	10.090	0.00071	425	4pσ′(a′)			9.652	15.39
$^1A''$	10.178	0.00239	316	4dσ(a′)			9.80(7)	13.23
$^1A'$	10.230	0.00069	339	4dπ(a″)				
$^1A''$	10.251	0.00012	416	4dσ′(a′)			9.892	13.84

$^1A''$	10.298	0.00167	747	5pσ(a′)		10.06(7)	14.62
$^1A'$	10.342	0.03606	84		3pσ(a′)	10.253	14.08
$^1A''$	10.374	0.00369	761	5pσ′(a′)		10.13(6)	13.86
$^1A'$	10.382	0.00233	832	5pπ(a″)		10.115	14.27
$^1A''$	10.390	0.00920	213		3pπ(a′)		
$^1A''$	10.396	0.00049	332	4dσ″(a′)			
$^1A'$	10.418	0.00317	293	4dπ′(a″)		9.97(0)	14.39
$^1A''$	10.503	0.00017	1173	5sσ(a′)		10.018	14.21
$^1A''$	10.594	0.00009	1328	6pσ(a′)		10.32(9)	12.97
$^1A''$	10.669	0.00043	1102	6pσ′(a′)		10.386	13.61
$^1A'$	10.691	0.00387	1044	6pπ(a″)		10.36(7)	12.58
$^1A''$	10.763	0.00341	1230	6sσ(a′)		10.31(5)	13.81
$^1A''$	10.787	0.00376	212	5dσ′(a′)		10.253	14.08
$^1A''$	10.939	0.01096	285	5dσ″(a′)			
$^1A'$	11.003	0.01146	114		3dσ(a′)	10.75(0)	15.39
$^1A''$	11.025	0.00109	658	7pσ(a′)		10.488	13.75
$^1A''$	11.137	0.00020	316	7pσ′(a′)		10.51(4)	13.26
$^1A'$	11.169	0.00230	149		3dσ′(a′)		
$^1A'$	11.203	0.01757	289	6dπ′(a″)		10.454	13.45
$^1A''$	11.232	0.00452	126		3dπ(a′)		
$^1A'$	11.291	0.00382	171		4sσ(a′)		
$^1A''$	11.321	0.00644	539				
$^1A''$	11.362	0.00110	145		3dπ′(a′)		
$^1A'$	11.379	0.00270	466	7pπ(a″)			

$^1A'$	11.400	0.00146	166		3dσ″(a′)	
$^1A'$	11.487	0.03372	196			HOMO-1 → 4sσ(a′) + HOMO-2 → 3sσ/σ*(OH)
$^1A'$	11.551	0.00433	153			HOMO-2 → 3sσ/σ*(OH) + HOMO-1 → 4sσ(a′)
$^1A'$	11.654	0.01614	302		4pσ(a′)	
$^1A''$	11.665	0.01108	311	7pσ(a′)		
$^1A''$	11.710	0.02432	330	8sσ(a′)		
$^1A''$	11.839	0.01799	144			HOMO → 7sσ(a′) + HOMO-3 → 3sσ/σ*(OH)
$^1A'$	11.904	0.00239	429		5sσ(a′)	
$^1A'$	11.951	0.01483	201			HOMO → 6dπ(a″) + HOMO-1 → 4dσ(a′)
$^1A'$	12.025	0.00078	289		4dσ(a′)	
$^1A'$	12.041	0.00006	402			HOMO → 6dπ(a″) + HOMO-1 → 4dσ′(a′)
$^1A'$	12.090	0.00622	683			HOMO → 6dπ(a″) + HOMO-1 → 4dσ′(a′)
$^1A'$	12.149	0.01876	797		4pσ′(a′)	
$^1A'$	12.188	0.00170	326		4dσ″(a′)	
$^1A'$	12.265	0.04963	660			HOMO-1 → 5sσ(a′) + HOMO → 7pσ′(a′)
$^1A'$	12.323	0.03324	839		5pσ(a′)	

[a] Mean value of r^2 (electronic radial spatial extents)

Table 3. The calculated vertical excitation energies of CH_3OH, compared with our experimental data and the results from previous work (energies in eV). See text for details.

State	Exp. (eV)	EOM-CCSD aug-cc-PVQZ+R	TD-LC-ωPBE aug-cc-PVQZ+R	Assignment	Buenker et al.[54] MRD-CI/DZP+R	Cheng et al.[22] TD-B3LYP cc-pVTZ	Cheng et al.[22] TD-B3LYP cc-pVQZ	Cheng et al.[22] TD-B3LYP cc-pV5Z
1 $^1A''$	6.757	6.948	6.9263	2a″→ 3sσ/σ*(OH)	6.84	6.975	6.780	6.576
2 $^1A''$	7.727	8.136	8.1289	2a″→ 3pσ(a')/σ*(CH)	7.92	8.187	7.920	7.635
2 $^1A'$	8.318	8.573	8.4237	2a″→ 3pπ(a″)		9.373	9.108	8.603
3 $^1A''$	8.449	8.592	8.4293	2a″→ 3pσ'(a')		9.552	9.234	8.613
3 $^1A'$	9.38(3)	8.904	8.7245	7a′ → 3sσ/σ*(OH)	9.97	8.761	8.525	8.300
4 $^1A'$	9.635	9.635	9.6220	7a′ → 3pσ(a′)/σ*(CH) + 2a″ → 4pπ (a″)		9.928	9.611	9.289
4 $^1A''$	8.907	9.197	9.0124	2a″→ 3dσ(a')/σ*		10.199	9.766	9.345
5 $^1A''$	9.088	9.365	9.2218	2a″→ 3dσ'(a')		…	…	…

the last decimal of the experimental energy value is given in brackets for this less-resolved features.

Table 4. Proposed vibrational assignments of the CH_3OH absorption bands in the photon energy range 7.5−9.1 eV[a]. Energies in eV.

		This work					Previous work	
assignment	energy	ΔE (υ_1')	ΔE (υ_6')	ΔE (υ_7')	ΔE (υ_8')	ΔE (υ_{11}')	ref.[22]	ref.[25]
$3p\sigma/\sigma^*_{CH} \leftarrow n_O(2a'')$								
0_0^0	7.727	…	…	…	…		7.727	7.722
7_0^1	7.798	…	…	0.071	…		7.798	7.803
8_0^1	7.827	…	…	…	0.100		7.827	7.825
6_0^1	7.857	…	0.130	…	…		7.862	7.862
8_0^2 / $7_0^1+6_0^1$	7.925	…	0.127	…	0.098		7.921	7.919
$8_0^1+6_0^1$	7.94(8)(s)	…	0.121	…	…		7.951	…
6_0^2	7.99(6)(s)	…	0.139	…	…		…	…
$7_0^1+6_0^2$	8.05(4)(b)	…	0.129	…	…		…	…
$8_0^1+6_0^2$	8.08(0)(s)	…	0.132	…	…		…	…
1_0^1	8.135	0.408	…	…	…		8.139	…
$8_0^1+6_0^3$	8.20(0)(s,w)	…	0.120	…	…		…	…
$3p\pi \leftarrow n_O(2a'')$								
0_0^0	8.318	…	…	…	…	…	8.313	8.321
7_0^1	8.38(3)(s)	…	…	0.065	…	…	…	…
8_0^1	8.42(3)(s)	…	…	…	0.105	…	…	8.443
11_0^1	8.449	…	…	…	…	0.131	…	…
$7_0^1+11_0^1$	8.50(4)(s)	…	…	…	…	0.121	…	…
$11_0^1+8_0^1$	8.55(6)(s)	…	…	…	0.107	…	…	…
11_0^2	8.57(5)(b)	…	…	…	…	0.126	…	8.568
$7_0^1+11_0^1+8_0^1$	8.60(1)(s)	…	…	…	0.097	…	…	…
$7_0^1+11_0^2$	8.63(1)(s)	…	…	…	…	0.127	…	…
$11_0^2+8_0^1$	8.68(5)(w)	…	…	…	0.110	…	…	…
11_0^3	8.71(3)(b)	…	…	…	…	0.138	…	…
$7_0^1+11_0^2+8_0^1$	8.741	…	…	…	0.110	…	…	…
$7_0^1+11_0^3$	8.75(3)(b)	…	…	…	…	0.122	…	…
$7_0^1+11_0^3+8_0^1$	8.87(5)(b)	…	…	…	0.122	…	…	…
$3d\sigma/\sigma^*_{CH} \leftarrow n_O(2a'')$								
0_0^0	8.907	…	…	…	…		…	8.756
7_0^1	8.968	…	…	0.061	…		…	…
8_0^1	9.01(1)(b)	…	…	…	0.104		…	…

[a] (s) shoulder structure; (b) broad structure; (w) weak feature (the last decimal of the energy value is given in brackets for these less-resolved features);

Table 5. Proposed assignments of vibrational progressions in CH_3OH absorption bands in the photon energy range 8.2−8.9 eV[a]. Energies in eV.

This work					Previous work
assignment	energy	ΔE (υ_{11}')	assignment	ΔE (υ_{12}')	Ref.[22]
$3p\pi \leftarrow n_O(2a'')$					
11^n	8.21(1)(w)	…	…	…	…
11^{n+1}	8.34(4)(s)	0.133	…	…	8.328
11^{n+2}	8.46(9)(s)	0.125	…	…	8.471
11^{n+3}	8.60(1)(s)	0.132	…	…	…
11^{n+4}	8.741	0.140	…	…	8.726
11^{n+5}	8.87(5)(b)	0.134	…	…	8.869
11^n	8.24(4)(s)	…	12^n	0.033	8.240
11^{n+1}	8.38(3)(s)	0.139	12^{n+1}	0.039	…
11^{n+2}	8.50(4)(s)	0.121	12^{n+2}	0.035	…
11^{n+3}	8.63(1)(s)	0.127	12^{n+3}	0.030	…
11^{n+4}	8.75(3)(b)	0.122	…	…	…
11^n	8.268	…	12^n	0.024	8.262
11^{n+1}	8.40(3)(s)	0.135	12^{n+1}	0.020	8.443
11^{n+2}	8.54(5)(s,b)	0.142	12^{n+2}	0.041	…
11^{n+3}	8.67(3)(s,w)	0.128	12^{n+3}	0.042	…
11^n	8.296	…	12^n	0.028	8.289
11^{n+1}	8.42(3)(s)	0.127	12^{n+1}	0.020	8.421
11^{n+2}	8.55(6)(s)	0.133	12^{n+2}	0.011	8.567
11^{n+3}	8.68(5)(w)	0.129	…	…	…

[a] (w) weak feature; (s) shoulder structure; (b) broad structure (the last decimal of the energy value is given in brackets for these less-resolved features);

Table 6. Proposed assignments of vibrational progressions in CH_3OH absorption bands in the photon energy range 9.0−10.8 eV[a]. Energies in eV.

This work				
assignment	energy	ΔE (υ_7')	ΔE (υ_8')	ΔE (υ_{12}')
$3d\sigma'(2a'')^{-1}$	9.088	…	…	…
$3d\sigma' + 12_0^1$	9.12(4)(s,b)	…	…	0.036
$3d\sigma' + 7_0^1$	9.164	0.076	…	…
$3d\pi'(2a'')^{-1}$	9.238	…	…	…
$3d\pi' + 7_0^1$	9.31(6)(s)	0.078	…	…
$3d\pi' + 8_0^1$	9.34(0)(s)	…	0.102	…
$3d\pi' + 7_0^1 + 8_0^1$	9.42(3)(s)	…	0.107	…
$3d\pi' + 7_0^1 + 8_0^2$	9.53(4)(s)	…	0.111	…
$4s\sigma(2a'')^{-1}$ / $3s\sigma(7a')^{-1}$	9.38(3)(b)	…	…	…
$4s\sigma + 7_0^1$ / $3s\sigma + 7_0^1$	9.45(6)(s)	0.073	…	…
$4p\sigma(2a'')^{-1}$	9.50(2)(b)	…	…	…
$4p\sigma + 7_0^1$	9.58(2)(s)	0.080	…	…
$4p\pi(2a'')^{-1}$	9.635	…	…	…
$4p\pi + 8_0^1$	9.741	…	0.106	…
$4p\pi + 8_0^2$	9.849	…	0.108	…
$4p\sigma'(2a'')^{-1}$	9.652	…	…	…
$4p\sigma' + 8_0^1$	9.763	…	0.111	…
$4p\sigma' + 8_0^1 + 7_0^1$	9.839	0.076	…	…
$4d\sigma(2a'')^{-1}$	9.80(7)(b)	…	…	…
$4d\sigma + 8_0^1$	9.914	…	0.107	…
$4d\sigma'(2a'')^{-1}$	9.892	…	…	…
$4d\sigma' + 8_0^1$	9.992	…	0.100	…
$4d\sigma' + 8_0^2$	10.108	…	0.116	…
$3p\sigma(7a')^{-1}$	9.941	…	…	…
$3p\sigma + 8_0^1$	10.06(2)(s)	…	0.121	…

$5p\sigma(2a'')^{-1}$	10.06(7)(b)	…	…	…
$5p\sigma + 7_0^1$	10.143	0.076	…	…
$5p\sigma + 8_0^1$	10.17(3)(s)	…	0.106	…
$5p\sigma + 8_0^2$	10.264	…	0.091	…
$5p\pi(2a'')^{-1}$	10.10(8)(s)	…	…	…
$5p\pi + 8_0^1$	10.226	…	0.118	…
$6p\pi(2a'')^{-1}$	10.36(7)(s)	…	…	…
$6p\pi + 7_0^1$	10.428	0.061	…	…
$9p\sigma(2a'')^{-1}$	10.644	…	…	…
$9p\sigma + 8_0^1$ / $3d\sigma(7a')^{-1}$	10.75(0)(b)	…	0.106	…

[a] (s) shoulder structure; (b) broad structure; (w) weak feature (the last decimal of the energy value is given in brackets for these less-resolved features);

Table 7. Energy values (eV), quantum defects (δ) and our assignments of the Rydberg series converging to the ionic electronic ground $(2a'')^{-1}$ and first $(7a')^{-1}$ excited states of methanol, CH_3OH[a].

This work			Ref.[22]	Ref.[31]
E_n	δ	assignment	E_n	E_n
IE_1 = 10.846 eV[b] $(2a'')^{-1}$				
($ns\sigma \leftarrow 2a''$)				
6.757	1.17	3sσ	6.760	6.739
9.38(3)(b)	0.95	4sσ	–	–
10.018	0.95	5sσ	–	–
10.31(5)(s)	0.94	6sσ	–	–
10.47(2)(b)	0.97	7sσ	–	–
10.57(5)(s)	0.91	8sσ	–	–
10.63(7)(s)	0.93	9sσ	–	–
10.67(9)(s)	0.97	10sσ	–	–
($np\sigma \leftarrow 2a''$)				
7.727	0.91	3pσ	7.727	7.721
9.50(2)(b)	0.82	4pσ	9.498	–
10.06(7)(b)	0.82	5pσ	10.065	–
10.32(9)(s)	0.87	6pσ	10.356	–
10.488	0.83	7pσ	–	–
10.584	0.79	8pσ	–	–
10.644	0.79	9pσ	–	–
10.688	0.72	10pσ	–	–
($np\pi \leftarrow 2a''$)				
8.318	0.68	3pπ	8.313	–
9.635	0.65	4pπ	9.627	–
10.10(8)(s)	0.70	5pπ	10.139	–
10.36(7)(s)	0.67	6pπ	10.377	–
10.50(4)(s,w)	0.69	7pπ	–	–
($np\sigma' \leftarrow 2a''$)				
8.449	0.62	3pσ′	8.313	–

9.652	0.62	4pσ′	9.627	–
10.13(6)(w)	0.62	5pσ′	10.139	–
10.386	0.56	6pσ′	10.377	–
10.51(4)(s)	0.60	7pσ′	–	–
10.59(7)(s,w)	0.61	8pσ′	–	–
(*ndσ ← 2a″*)				
8.907	0.35	3dσ	8.899	–
9.80(7)(b)	0.38	4dσ	9.826	–
10.20(0)(w)	0.41	5dσ	10.215	–
10.41(5)(s)	0.38	6dσ	10.419	–
(*ndσ′ ← 2a″*)				
9.088	0.22	3dσ′	9.068	–
9.892	0.22	4dσ′	9.902	–
10.253	0.21	5dσ′	10.247	–
10.43(6)(s)	0.24	6dσ′	10.446	–
10.545	0.27	7dσ′	10.562	–
(*ndπ′ ← 2a″*)				
9.238	0.09	3dπ′	9.235	9.237
9.97(0)(s)	0.06	4dπ′	9.988	–
10.27(9)(s)	0.10	5dπ′	10.297	–
10.454	0.11	6dπ′	10.466	–
10.57(5)(s)	0.09	7dπ′	10.575	–
IE_2 = 12.62 eV[c] $(7a')^{-1}$				
(*nsσ ← 7a′*)				
9.38(3)(b)	0.95	3sσ	8.103[d]	–
(*npσ ← 7a′*)				
9.941	0.75	3pσ	–	–
(*npσ′ ← 7a′*)				
10.253	0.60	3pσ′	–	–
(*ndσ ← 7a′*)				
10.75(0)(b)	0.30	3dσ	–	–

[a] (b) broad structure; (s) shoulder structure; (w) weak feature (the last decimal of the energy value is given in brackets for these less-resolved features); [b] adiabatic value from ref.[32]; [c] vertical value from ref.[31]; [c] calculated value.

TOC Graphic